JGR Atmospheres

RESEARCH ARTICLE
10.1029/2019JD031849

The Impact of Continuing CFC-11 Emissions on Stratospheric Ozone

Eric L. Fleming[1,2], Paul A. Newman[1], Qing Liang[1], and John S. Daniel[3]

[1]NASA Goddard Space Flight Center, Greenbelt, MD, USA, [2]Science Systems and Applications, Inc., Lanham, MD, USA, [3]Chemical Sciences Division, Earth System Research Laboratory, National Oceanic and Atmospheric Administration, Boulder, CO, USA

Key Points:
- Continuing global CFC-11 emissions at 2013–2016 average levels of 72.5 Gg/year will have a substantial impact on future stratospheric ozone
- The time-integrated ozone depletion has a strong linear dependence on the cumulative amount of CFC-11 emissions
- The sensitivity of the ozone response to CFC-11 has a modest inverse dependence on future CO_2, CH_4, and N_2O concentrations

Correspondence to:
E. L. Fleming,
eric.l.fleming@nasa.gov

Citation:
Fleming, E. L., Newman, P. A., Liang, Q., & Daniel, J. S. (2020). The impact of continuing CFC-11 emissions on stratospheric ozone. *Journal of Geophysical Research: Atmospheres*, *125*, e2019JD031849. https://doi.org/10.1029/2019JD031849

Received 18 OCT 2019
Accepted 7 JAN 2020
Accepted article online 10 JAN 2020

Abstract Trichlorofluoromethane (CFC-11, $CFCl_3$) is a major anthropogenic ozone-depleting substance and greenhouse gas, and its production and consumption are controlled under the Montreal Protocol. However, recent studies show that CFC-11 emissions have been near constant or increasing since 2002. In this study, we use a two-dimensional chemistry-climate model to investigate the stratospheric ozone response to a range of future CFC-11 emissions scenarios. A scenario with future emissions sustained at 10 gigagrams per year (Gg/year) above the baseline WMO (2018) A1 scenario results in minor additional global (90°S–90°N) ozone depletion of 0.13% by 2100, and a 1.5-year delay in the global ozone recovery to 1980 levels, relative to the baseline. A scenario with 72.5 Gg/year (the 2013–2016 average) sustained to 2100 results in a substantial 15% increase in effective equivalent stratospheric chlorine and nearly 1% additional global ozone depletion by 2100, with a 7.5-year delay in the recovery to 1980 global ozone levels, relative to the baseline. The ozone response averaged over time has a strong linear dependence on the cumulative amount of future CFC-11 emissions under a wide range of scenarios. The resulting ozone response sensitivity gives a simple metric relating the time-averaged ozone change to the cumulative CFC-11 emissions. This sensitivity has an inverse dependence on future greenhouse gas concentrations (CO_2, CH_4, and N_2O). For the medium Intergovernmental Panel on Climate Change Representative Concentration Pathway-6.0 scenario, the sensitivity per 1,000 Gg of cumulative CFC-11 emissions is −0.1% and −1% for global and Antarctic spring ozone, respectively.

Plain Language Summary Stratospheric ozone protects the Earth's biosphere from harmful ultraviolet radiation and is key in determining the radiative balance of the atmosphere. CFC-11 is a man-made chlorofluorocarbon, and its emissions and subsequent break down in the stratosphere result in ozone depletion. Because of this, production and consumption of CFC-11 have been controlled under the Montreal Protocol, resulting in a rapid decline in emissions starting in the late 1980s. Recent studies show that CFC-11 emissions have increased in recent years, at odds with expected declines caused by the Montreal Protocol controls. In this study, we examine how potential future CFC-11 emissions will impact stratospheric ozone. The ozone response is proportional to the amount of CFC-11 emitted, and the response is substantial for a future projection in which the increased emissions during 2013–2016 continue to 2100. This scenario will postpone the return of global ozone to 1980 levels from mid-2052 to 2060 and causes additional 1% global ozone depletion by 2100, compared to the baseline. Although there is uncertainty in projecting future emissions, the ozone response is strongly dependent on the amount of CFC-11 emissions accumulated over time, allowing for a simple metric relating the ozone depletion to the cumulative amount of emissions.

1. Introduction

Chlorofluorocarbons (CFCs) are both powerful ozone-depleting substances (ODSs) and greenhouse gases (GHGs). One of the most abundant CFCs is trichlorofluoromethane (CFC-11, $CFCl_3$), which historically had a variety of industrial uses: as a solvent and cleaning agent, as a propellant in aerosol spray cans, as the refrigerant in refrigeration and air conditioning applications, and as the blowing agent in foams. Because of its large impact on the ozone layer, CFC-11 production and consumption have been controlled under the Montreal Protocol, resulting in a dramatic decline in emissions starting in the late 1980s (Cunnold et al., 1997).

CFC-11 is removed in the stratosphere primarily by UV photolysis at 190–230 nm (98%) and to a lesser extent by gas-phase reaction with $O(^1D)$ atoms (2%). The current best estimate total lifetime and 1σ uncertainty for CFC-11 is 52 years (40–70 years) (SPARC, 2013). As a result of the Montreal Protocol and subsequent post-1980s emissions decrease, and the 52-year lifetime, tropospheric concentrations of CFC-11 peaked in about 1994 (WMO, 1999) and have declined up to the present.

Although CFC-11 emissions declined from the late 1980s to the early 2000s, they were fairly constant during 2002–2012. Montzka et al. (2018) showed that emissions then increased during 2013–2016, to an average of approximately 72.5 gigagrams per year (Gg/year) (as updated in Engel & Rigby, 2018; see also Prinn et al., 2018). Global emissions during 2014–2016 were roughly 10 Gg/year (~15%) higher than the 2002–2012 average, and significantly larger than 2006 and 2012 projections based on reported production and estimates of the bank and bank release fraction (see Engel & Rigby, 2018). The 2013–2106 emissions increase was likely not explained by release from existing CFC-11 banks. While the origin of the increase was not identified, Montzka et al. suggested that the emissions most likely originated from eastern Asia. The subsequent study of Rigby et al. (2019) showed that at least 40–60% of the increase in global emissions, roughly 7 Gg/year, originated from eastern China. The Montzka et al. and Rigby et al. studies suggest that the emissions increase was associated with new production and consumption not reported to the United Nations Environment Programme.

Because of the recent emissions increase, long residence time in the atmosphere, and significant potential to deplete ozone, it is important to understand and quantify the stratospheric ozone response to potential future CFC-11 emissions increases. In this paper, we calculate the stratospheric ozone impact due to a range of future CFC-11 emissions scenarios, including those based on Montzka et al. (2018). We quantify the increase in equivalent effective stratospheric chlorine (EESC) and estimate the delays in the recovery of EESC and ozone due to additional CFC-11 emissions. We also examine the relationship between the time-integrated ozone response and the cumulative amount of emissions over the 2017–2100 time period under a range of greenhouse gas scenarios, with a brief examination of the ozone response beyond 2100.

2. Model Simulations and Scenarios

Simulations in this study are conducted with the National Aeronautics and Space Administration (NASA)/Goddard Space Flight Center two-dimensional model (GSFC2D), which has been used in chemistry-climate coupling studies of the stratosphere and mesosphere as well as the World Meteorological Organization ozone assessments, including WMO (2018). The model has full stratospheric chemistry, and its computational efficiency makes it a very useful tool for performing numerous sensitivity tests. The model has undergone extensive improvement and evaluation over the years (e.g., Bacmeister et al., 1995; Considine et al., 1994; Fleming et al., 2007, 2011, 2015; Jackman et al., 1996, 2016; Rosenfield et al., 1997, 2002) and is shown to provide realistic ozone responses to chlorine perturbations. A model description and evaluation of the baseline simulation of CFC-11 and ozone is provided in Appendix A.

Given the uncertainty in future CFC-11 emissions, we examine the future stratospheric ozone response to CFC-11 using several global emission scenarios shown in Figure 1a. These scenarios are not meant to be predictions, but are formulated to examine impacts from plausible future emissions pathways, with the intent of generalizing the ozone responses to various levels of future cumulative emissions. The baseline (black line) follows the latest WMO (2018) A1 mixing ratio scenario (Carpenter & Daniel, 2018). Here historic emissions (1950–2016) are derived from global mixing ratio observations using a global 1-box model (Velders & Daniel, 2014) and a fixed lifetime of 52 years (SPARC, 2013). Future emissions (2017–2100) are projected to decay 6.4%/year; this assumes no new production and a bank release rate of 6.4%/year based on estimates of the amount of CFC-11 in existing equipment or applications (Carpenter & Daniel, 2018).

As discussed in Engel and Rigby (2018), recent trends inferred from the global surface observation networks show that emissions derived for 2014–2016 were ~10 Gg/year (~15%) higher than those derived for 2002–2012. This increase is not likely due to increasing emissions from banks and may indicate new production not reported to the United Nations Environment Programme. To account for this trend continuing into the future, we include a scenario in which the emissions are held at a constant 10 Gg/year above the baseline throughout 2017–2100 (Figure 1a, orange line). This assumes that the 10-Gg/year increase is a constant delta above a steadily decreasing background emission.

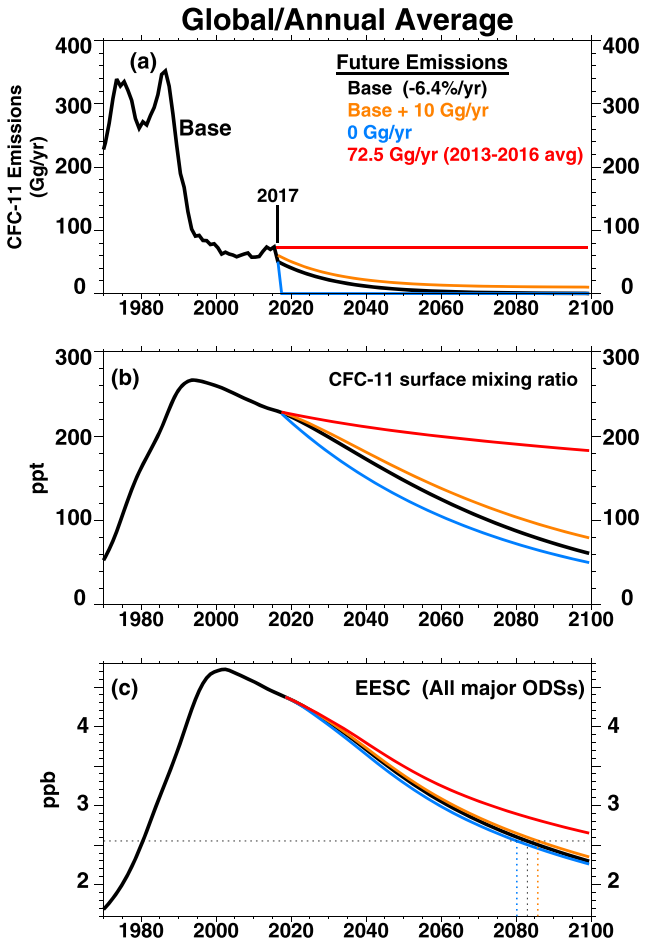

Figure 1. Time series of global (90°S–90°N) and annual average (a) CFC-11 surface emissions (Gigagrams (Gg)/year); (b) CFC-11 surface mixing ratio (parts per trillion, ppt); and (c) equivalent effective stratospheric chlorine (EESC, in parts per billion, ppb) at 50 km (0.8 hPa), for the four future CFC-11 emission scenarios listed in Table 1. Included are the baseline scenario (black), baseline +10 Gg/year sustained for 2017–2100 (orange); zero emissions for 2017–2100 (blue), and 72.5 Gg/year sustained for 2017–2100 (red). All scenarios are identical to the baseline prior to 2017. Also shown are the EESC return dates to 1980 values (vertical dashed lines).

As discussed above regarding the A1 scenario, future emissions of CFC-11 are projected to decrease from present day, assuming compliance with the Montreal Protocol and assuming that bank fractional release amounts remain roughly constant over time (WMO, 2018). However since 2002, the actual inferred emissions from atmospheric observations have been fairly constant or increasing. The length of time that such an "excess" emission would occur and the magnitude of this emission will depend on how long production continues, how much is produced, and how much of the production is released quickly to the atmosphere as opposed to, for example, being retained inside insulating foams. If these new emissions are associated with uses that substantially increase the CFC-11 banks, larger emissions resulting from this new production would be expected in the future (Engel & Rigby, 2018). Therefore, we include a scenario that assumes the 2013–2016 inferred average of 72.5 Gg/year (WMO, 2018) will be sustained out to 2100 (Figure 1a, red line). This emission level is slightly higher (by ~8%) than the longer term 2002–2016 inferred average of 67 Gg/year (Carpenter & Daniel, 2018; Engel & Rigby, 2018). Finally, we include a scenario of zero emissions for 2017–2100 (Figure 1a, blue line; see also Table 1). While this serves as the absolute lower limit of the future CFC-11 impact, zero future emissions is a highly idealized scenario since it is unlikely that all CFC-11 banks will be recovered and some future emissions would still be expected. Prior to 2017, all scenarios are identical to the baseline, where the model is forced with the global surface mixing ratios from the A1 scenario (Figure 1b, black line).

Table 1
Future CFC-11 Emission Scenarios (2017–2100) Shown in Figures 1 and 2

Scenario	Future emissions (2017–2100)	EESC	Global/annual avg ozone			Antarctic spring ozone[b]		
			change from base		Return to 1980 level	Change from base		
		Return to 1980 level	2060	2100		2060	2100	Return to 1980 level
Base[a]	6.4%/year decay	2083.0	-	-	2052.5	-	-	2070.5
Lower limit	0 Gg/year	2080.2 (−2.8 years)	+0.16%	+0.09%	2050.8 (−1.7 years)	+1.4%	+0.70%	2068.3 (−2.2 years)
Base +10	Base+10 Gg/year	2085.8 (+2.8 years)	−0.09%	−0.13%	2054.0 (+1.5 years)	−0.81%	−1.1%	2073.7 (+3.2 years)
2013–2016 Avg	72.5 Gg/year	2108.4[c] (+25.4 years)	−0.50%	−0.89%	2060.0 (+7.5 years)	−4.3%	−7.1%	2095.1 (+24.6 years)

Note. Also shown are the dates of return to 1980 values for EESC (equivalent effective stratospheric chlorine), the percentage change from the baseline in 2060 and 2100, and the date of return to 1980 values for global/annual average and Antarctic spring total column ozone. The difference from the baseline of the return dates is shown in parentheses. The EESC and ozone values are from simulations that use the IPCC RCP6.0 GHG scenario.
[a]From WMO (2018). [b]Antarctic spring is defined as the average over 90°S-65°S for September–October. [c]Determined by extrapolating beyond 2100.

To test the linearity of the ozone response, we ran several additional emissions scenarios for 2017–2100: (1) a "medium" scenario of sustained 30 Gg/year (roughly one-half of the inferred emissions during 2002–2016); (2) sustained 64 Gg/year (the 2002–2012 average inferred by Montzka et al., 2018 and WMO, 2018); and (3) a very high scenario of sustained 100 Gg/year. Finally, to test the near- and long-term time dependence of the ozone response, we ran three additional scenarios with identical total emissions but different emissions time dependence in the near-term future. These will be discussed in section 3.4.

For the other long-lived ODSs, the WMO (2018) A1 scenario is used for all simulations. We note that the recent emissions increase of CFC-11 may be related to emissions changes of other ODSs such as CFC-12 (CCl_2F_2) and CCl_4 (e.g., from feedstock uses). However, in this paper we focus on the impacts due to only CFC-11 emissions. For CO_2, CH_4, and N_2O, the Intergovernmental Panel on Climate Change (IPCC) Representative Concentration Pathways (RCP) medium Scenario 6.0 ("historic" scenario before 2005, Meinshausen et al., 2011) is used for the simulations shown in Figures 1–5. In section 3.3, we explore the impact of different GHG scenarios on the ozone response.

3. Results

3.1. EESC and Ozone Responses

Figure 1 shows the 1970–2100 global (90°S–90°N) and annual average (b) CFC-11 surface concentration and (c) EESC for the four emissions scenarios shown in Figure 1a and listed in Table 1. Here EESC is taken as the sum of the model inorganic chlorine plus 60 times the inorganic bromine from all long-lived ODSs in the global upper stratosphere (1 hPa, ~48 km), following Newman et al. (2007). Figure 2 shows the corresponding total ozone responses for the (a) global/annual average and (b) Antarctic spring. For context, we include the historical ground-based total ozone observational data record (1964–2017) in Figures 2a and 2b. We note that unlike 3-D chemistry-climate models, the inherent interannual variability in GSFC2D is negligible so that the long-term model time series are very smooth in Figures 1b and 1c, and 2.

The future surface mixing ratio of the baseline scenario calculated in GSFC2D (Figure 1b, black line) is slightly larger than the A1 scenario calculated from the global 1-box model (Carpenter & Daniel, 2018), with a maximum difference of 5 parts per trillion (ppt) in 2065. This is due to the inherent model differences, including the constant 52-year lifetime assumed in the 1-box model versus the model calculated (i.e., time dependent) GSFC2D lifetime that is slightly longer than 52 years through most of the 21st century. The GSFC2D lifetime decreases from 55 years in 2000 to 50 years in 2100, with a 2000–2100 average of 53 years for RCP6.0 GHG conditions. Long-term changes in the CFC-11 lifetime will be discussed further in section 3.3.

Zeroing the future emissions (Figure 1b, blue line) results in a smaller surface concentration compared to the baseline (as expected), with a maximum difference of −22 ppt in 2044. By the latter 21st century, most of the CFC-11 emissions reduction is already achieved under the baseline scenario, so that with a 50- to 55-year

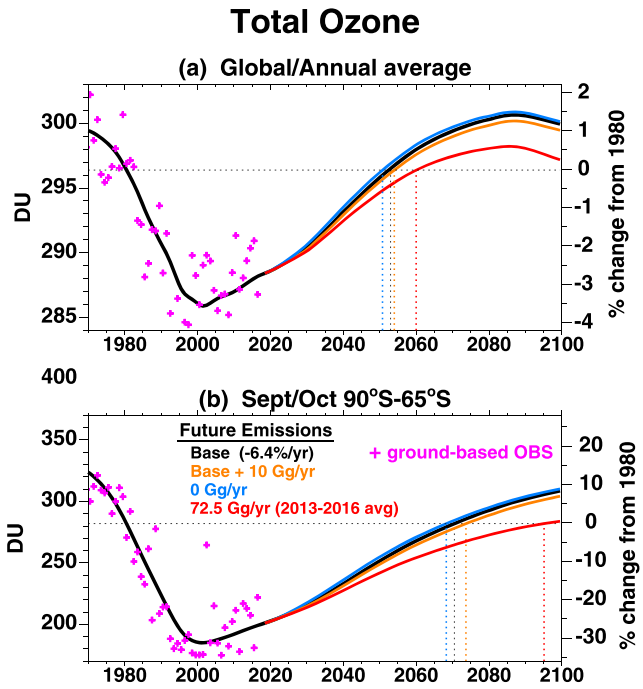

Figure 2. Total column ozone time series for the (a) global (90°S–90°N) and annual average and (b) Antarctic spring (September–October average for 65°S–90°S), given in Dobson Units (DU) and percent change from 1980 values, for the four future CFC-11 emission scenarios shown in Figure 1a and Table 1. Included are the baseline scenario (black), baseline +10 Gg/year sustained for 2017–2100 (orange); zero emissions for 2017–2100 (blue), and 72.5 Gg/year sustained for 2017–2100 (red). All scenarios are identical to the baseline prior to 2017. Also shown are the return dates to 1980 values (vertical dashed lines) and ground-based observations for 1964–2017 (magenta plus signs, updated from Fioletov et al., 2002). The model in Figure 2b has been offset by −30 DU to minimize differences with the observations in the 1970s and facilitate long-term model-data comparison.

lifetime, zeroing the future emissions has a smaller impact compared to the baseline by 2100, with a difference of −11 ppt. The EESC and ozone differences from the baseline are small (Figures 1c and 2), with an EESC reduction of 0.03–0.05 parts per billion (ppb) through the 21st century. By 2100, global and Antarctic spring ozone increase by ~0.1% and 0.7%, respectively, above the baseline. With zero future emissions, EESC and ozone return to 1980 levels 2–3 years earlier compared to the baseline (Table 1). This is similar to other long-lived ODSs, where zeroing future emissions resulted in a return to 1980 EESC levels of 1–3 years earlier than the baseline scenario (Carpenter & Daniel, 2018).

For the base +10 Gg/year scenario (Figures 1 and 2, orange line), the differences from the baseline increase throughout the 21st century, but the resulting perturbation is relatively small by 2100: +18 ppt in surface concentration and +0.05 ppb (+2%) in EESC. For global and Antarctic spring ozone, this results in additional ozone depletion of 0.13% and 1.1% in 2100, and a delay in the recovery to 1980 levels of 1.5 and 3.2 years, respectively.

The sustained 72.5 Gg/year scenario (Figures 1, 2, red line) substantially perturbs the stratosphere. CFC-11 surface concentrations significantly increase through the 21st century to be 125 ppt above the baseline by 2100, with a 0.35 ppb (15%) increase in EESC. This causes an ozone change that grows over time and eventually leads to additional ozone depletion greater than that caused by all future halocarbon ODS emissions in the baseline scenario (this is determined by comparing the baseline with a simulation that has zero future emissions for all ODSs— see Carpenter & Daniel, 2018). Relative to the baseline, the sustained 72.5 Gg/year scenario results in additional global ozone depletion of nearly 1% in 2100 and a delay in the recovery to 1980 levels of 7.5 years (Table 1). For Antarctic spring ozone, this 72.5 Gg/year scenario results in additional depletion of nearly 7% in 2100, with a delay in the recovery to 1980 levels of 24.6 years. The return to 1980 EESC levels does not occur until after 2100.

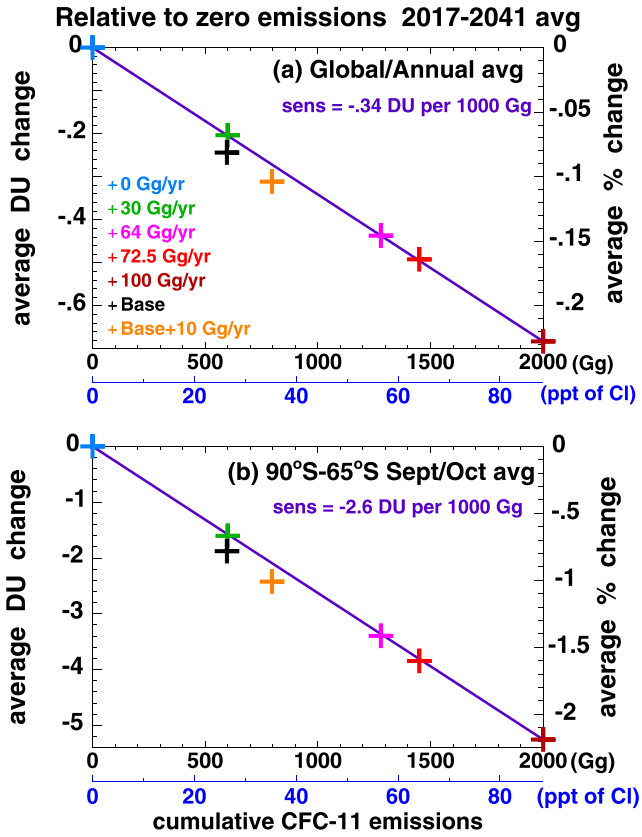

Figure 3. Cumulative CFC-11 emissions versus the average total ozone response for the four scenarios listed in Table 1 and the additional sensitivity scenarios described in section 2. Emissions are accumulated over 2017–2036, and the ozone response is averaged over an additional 5 years (2017–2041) to account for a 5-year time lag from emissions release at the surface and subsequent ozone depletion in the stratosphere. Results are taken relative to zero CFC-11 emissions for (a) the global (90°S–90°N) and annual average and (b) Antarctic spring ozone, using the RCP6.0 GHG scenario. The cumulative emissions are expressed in both gigagrams (Gg) and parts per trillion (ppt) of chlorine, with the conversion from mass to volume mixing ratio done as in the 1-box model (Velders & Daniel, 2014).

3.2. Sensitivity of the Ozone Response

The ozone change averaged over time has a strong linear dependence on the cumulative amount of future CFC-11 emissions. This is seen over the range of emission scenarios for total column and vertical profile ozone at all latitudes and altitudes. This point is consistent with the recent modeling study of Keeble et al. (2019), who found a robust linear relationship between the cumulative emissions and the response and timing of the recovery in total ozone. As an example, Figure 3 shows this linear dependence for the near-term future (2017–2041) for the four scenarios shown in Figures 1 and 2 and Table 1, and the additional sensitivity scenarios described in section 2. Here the emissions are accumulated over 20 years (2017–2036), and the ozone response is averaged over an additional 5 years (2017–2041) to include a 5-year time lag to account for the time delay between the emissions release at the surface and subsequent ozone depletion in the stratosphere. The ozone response is taken relative to the zero emissions scenario, and the cumulative emissions are expressed in both gigagrams and ppt of chlorine, with the conversion from mass to volume mixing ratio done as in the 1-box model (Velders & Daniel, 2014).

The scenarios with emissions constant in time yield a strong linear relationship with very little offset. The resulting sensitivity (linear slope) gives a simple metric relating the average ozone change to the cumulative CFC-11 emissions. For the 2017–2041 average, this relationship is −0.34 Dobson Units (DU) (−0.11%) and −2.6 DU (−1.0%) per 1,000 Gg cumulative CFC-11 emissions, for global/annual and Antarctic spring total ozone, respectively (Figure 3). For the base and base +10 Gg/year scenarios, the ozone sensitivity is slightly larger than this relationship (Figure 3, black and orange "+"). This is due to the small time dependence of

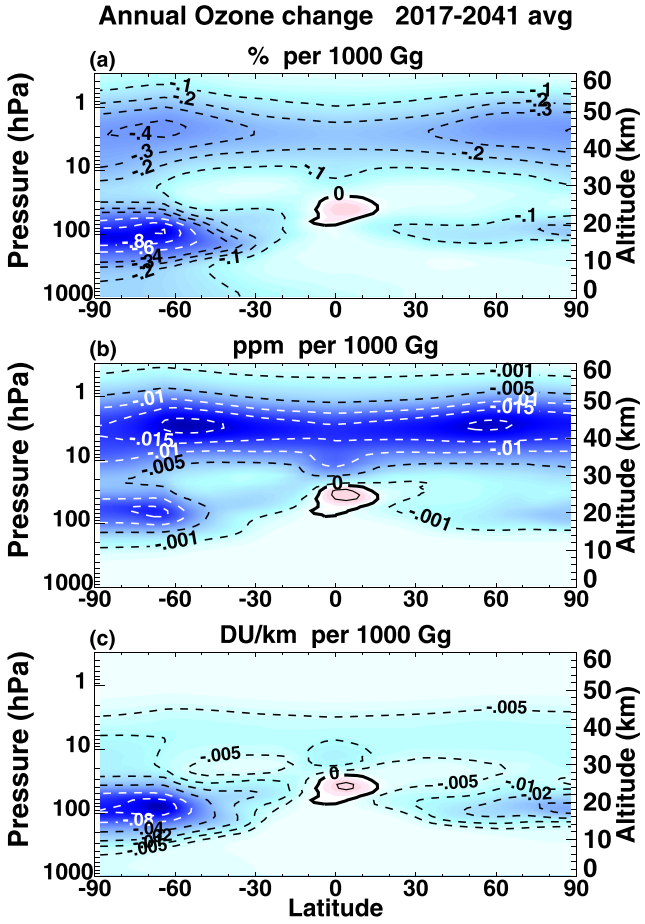

Figure 4. Annual ozone response to cumulative CFC-11 emissions averaged over 2017–2041. A 5-year lag from the emissions release at the surface is used for the ozone response, which is shown in (a) percent per 1,000 Gg, (b) ppm per 1,000 Gg, and (c) DU/km per 1,000 Gg cumulative emissions. The contour intervals are (a) −0.1 for values ≥−0.4 and include the −0.6, −0.8, and −1% per 1,000 Gg contours; (b) −0.005 and include the ±0.001 ppm per 1,000 Gg contours; (c) −0.04 and include the −0.02, −0.01, and ± 0.005-DU/km contours.

the emissions, as more CFC-11 is emitted earlier in the time period (Figure 1a), combined with the long lifetime (50–55 years), resulting in slightly more ozone depletion per gigagram compared to emissions that are constant with time.

The latitude-height distribution of the ozone sensitivity to additional CFC-11 is consistent with that expected due to chlorine perturbations (e.g., WMO, 1999, 2018). Figure 4 shows the annual ozone response averaged over 2017–2041 as in Figure 3, expressed as the change per 1,000 Gg of cumulative emissions. The largest ozone depletion occurs in the Antarctic lower stratosphere (−1% per 1,000 Gg) and in the upper stratosphere globally (−0.3 to −0.4% per 1,000 Gg). There is a secondary area of ozone loss of smaller magnitude in the Arctic lower stratosphere (−0.1 to −0.2% per 1,000 Gg). Also shown are the same changes expressed in different units (Figure 4b: mixing ratio, parts per million, ppm; Figure 4c: Dobson Units per km, DU/km), emphasizing the changes in the upper and lower stratosphere, respectively. Largest mixing ratio changes occur globally at 2–4 hPa (−0.02 ppm per 1,000 Gg); largest DU/km changes occur in the very lower polar stratosphere, especially in the Southern Hemisphere (SH, −0.1 DU/km per 1,000 Gg).

The largest total ozone losses from increased CFC-11 emissions occur in the polar regions. This is seen in Figure 5, where the largest total ozone changes occur in the polar spring in each hemisphere. The increased depletion in the Antarctic ozone hole is evident, with an additional 1.5% (3.5 DU) per 1,000 Gg of ozone loss at 80°S-90°S during October. However, additional ozone depletion of ~0.3% per 1,000 Gg persists throughout the year at SH polar latitudes. In the Northern Hemisphere (NH), the largest additional depletion of 0.15% per 1,000 Gg occurs in the polar late winter-early spring, with minor ozone loss of ~0.05% per 1,000 Gg in

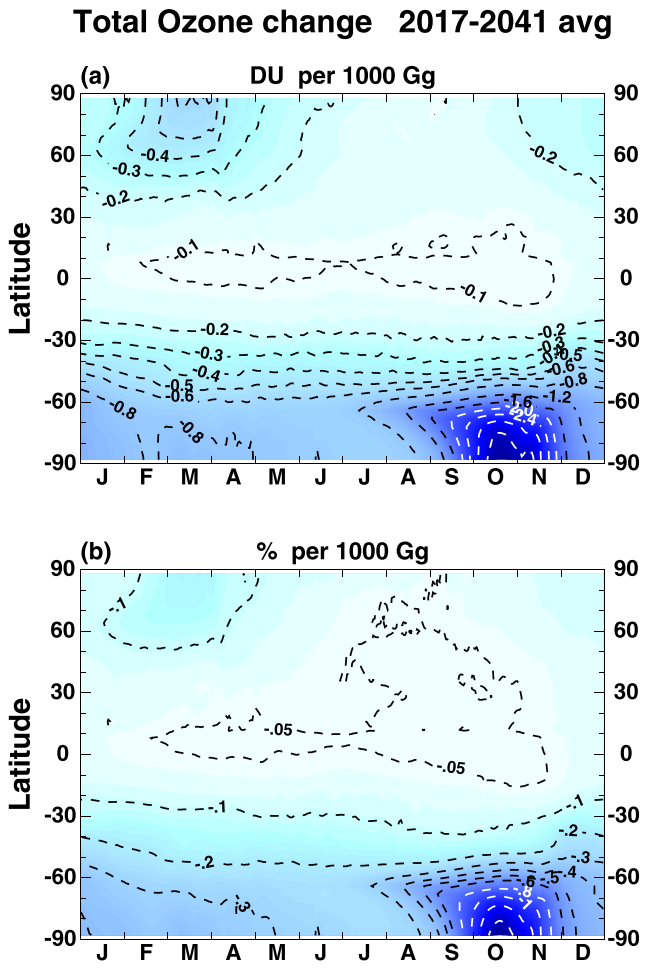

Figure 5. Season versus latitude total column ozone response to cumulative CFC-11 emissions averaged over 2017–2041. A 5-year lag from the emissions release at the surface is used for the total ozone response, which is shown in (a) Dobson units (DU) per 1,000 Gg and (b) percent per 1,000 Gg. The contour intervals are (a) −0.1 for values ≥−0.6 and −0.4 DU for values ≤−0.8 DU per 1,000 Gg; (b) −0.1 for values ≥−0.6 and −0.2 for values ≤−0.8 and include the −0.05% per 1,000 Gg contour.

the NH summer and fall, and in the tropics throughout the year. We note that ozone loss during Arctic winter-spring will have large year-to-year variability depending on the meteorology, with larger loss during cold winters. This effect is not captured in the current GSFC2D model, which computes essentially climatologically averaged transport fields.

A strong linear relationship between the cumulative emissions and the time-averaged ozone response, as shown in Figure 3, exists throughout the stratosphere regardless of the time period taken. However, the sensitivity (linear slope) is time dependent, as shown in Figure 6a for the global total and partial columns above and below 32 km (starting in 2022 since the ozone response is lagged by 5 years from the emissions release at the surface). Since the sensitivity is computed relative to the scenario in which emissions drop to zero starting in 2017, the time dependence reflects the adjustment of stratospheric chlorine and ozone depletion to zero emissions at the surface, as well as the slow decay of CFC-11 to zero concentration. As a result, the sensitivity throughout the stratosphere increases with time prior to the mid-2100s, with a slow decrease thereafter. For global total ozone, the sensitivity maximizes in ~2050 (−0.34 DU/1,000 Gg), with the column below and above 32 km contributing roughly 70% (−0.24 DU/1,000 Gg) and 30% (−0.1 DU/1,000 Gg), respectively. For Antarctic spring total ozone, the sensitivity is a maximum of −2.8 DU/1,000 Gg in the early 2060s (note that only the Antarctic total column response is shown in Figure 6b, as this is dominated by the region below 32 km, with only a very small contribution from the upper stratosphere, ~−0.1 DU). Changes in the background atmosphere will also impact the ozone sensitivity as discussed in the next section.

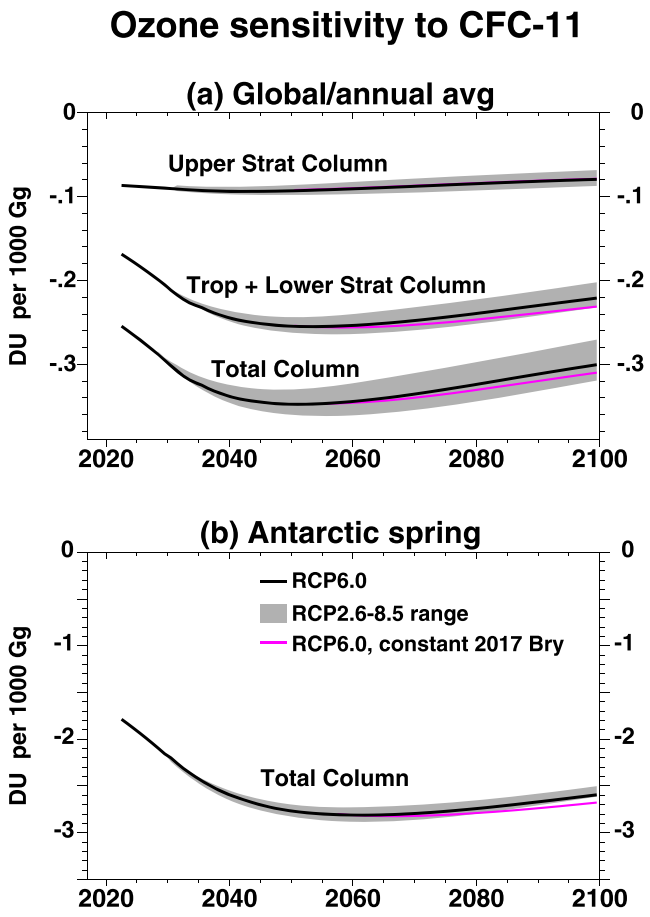

Figure 6. Sensitivity (in DU per 1,000 Gg) of the time-averaged ozone response, with a lag of 5 years, to the cumulative CFC-11 emissions for 2022–2100, taken relative to the zero emissions scenario. (a) Global (90°S–90°N) and annual average total column and partial columns for (1) the troposphere + lower stratosphere (below 32 km) and (2) upper stratosphere (above 32 km).(b) Antarctic spring total column. The black line shows results using the RCP6.0 GHG scenario. The gray shading depicts the range using the RCP2.6, RCP4.5, RCP6.0, and RCP8.5 GHG scenarios, with the largest sensitivity occurring under RCP2.6 (low GHG loading) and the smallest sensitivity occurring under RCP8.5 (high GHG loading). The magenta line shows results for the RCP6.0 GHG scenario, but with the bromine-containing source gases (CH_3Br and halons) fixed at 2017 levels (this simulation is nearly identical to the baseline for the global upper stratospheric column, Figure 6a, black).

3.3. Impact of GHGs and Bromine

The ozone response sensitivity in Figure 6 is dependent on the future concentration of GHGs (CO_2, CH_4, and N_2O). As discussed in previous studies, changing GHG loading can modify the future impact of chlorine perturbations on stratospheric ozone (e.g., see Pawson & Steinbrecht, 2014). This is done through modification of the chlorine-related catalytic ozone destruction by direct chemical perturbations or by changes to the radiative properties, temperature, and circulation of the stratosphere. First, increased NO_x from N_2O oxidation and increased CH_4 loading both mitigate the chlorine-ozone loss cycle by converting active chlorine to reservoir forms via the reactions:

$$ClO + NO_2 + M \rightarrow ClONO_2 + M \text{ (M is a third body)} \quad (1)$$

$$Cl + CH_4 \rightarrow HCl + CH_3 \quad (2)$$

Second, increased CO_2 concentrations: (a) accelerate the Brewer-Dobson circulation (BDC), thereby reducing the CFC-11 lifetime (Butchart & Scaife, 2001), and (b) cool the stratosphere, thereby reducing the ozone chemical loss rates (Haigh & Pyle, 1979). Both of these processes reduce the efficiency of chlorine-catalyzed

Table 2
Global and Antarctic Spring Total Ozone Response Sensitivity Per 1,000-Gg Cumulative CFC-11 Emissions Under Different RCP GHG Scenarios

GHG Scenario	Global annual ozone	Antarctic spring ozone[a]	CFC-11 lifetime in 2100 (years)
RCP 2.6	−0.32 DU (−0.11%)	−2.6 DU (−1.0%)	55.6
RCP 4.5	−0.31 DU (−0.10%)	−2.6 DU (−1.0%)	52.9
RCP 6.0	−0.30 DU (−0.10%)	−2.6 DU (−1.0%)	50.4
RCP 8.5	−0.27 DU (−0.09%)	−2.5 DU (−1.0%)	46.9

Note. The emissions are accumulated over 2017–2095, and the ozone response is averaged over an additional 5–years (2017–2100) to account for a 5-year time lag from the emissions release at the surface and subsequent ozone depletion in the stratosphere. Also shown is the CFC-11 lifetime in year 2100 (for reference, the lifetime is 55 years in 2000).
[a]Antarctic spring is defined as the average over 90°S-65°S for September–October.

ozone loss, although process (b) has only a small impact due to the weak temperature dependence of the chlorine-ozone reaction rates. In the polar region, stratospheric cooling may enhance ozone loss via the increase in polar stratospheric clouds, although this process may be at least partially offset by dynamically induced polar warming due to the BDC acceleration (e.g., see Dameris & Godin-Beekmann, 2014; Langematz & Tully, 2018). Reduction in the CFC-11 lifetime via process (a) is somewhat mitigated by long-term increases in the overhead ozone column, which increases the lifetime (Fleming et al., 2011; SPARC, 2013). The net impact of these processes reduces the CFC-11 lifetime in GSFC2D from 55 years in 2000 to 50 years in 2100 under the RCP6.0 scenario. In 2100, the CFC-11 lifetime has a range of 47–56 years across the RCP scenarios, with the lifetime becoming shorter with increasing GHG concentrations (Table 2).

The GHG loading also modifies stratospheric water vapor via increased CH_4 oxidation (e.g., Revell et al., 2016) and changes in the tropical tropopause temperature that largely controls the amount of H_2O entering the stratosphere (e.g., Karpechko & Maycock, 2018; Smalley et al., 2017). Any increase in stratospheric water vapor will increase polar stratospheric cloud formation and enhance the chlorine-induced ozone loss in the polar region. We note that GSFC2D captures these GHG-induced feedbacks either directly or through parameterizations, as described in Appendix A.

The net impact of CO_2, CH_4, and N_2O increases is to reduce the global ozone sensitivity to increased chlorine. This is shown in Table 2 for the response integrated over 2017–2100, as the global ozone sensitivity to increased CFC-11 emissions is inversely proportional to GHG loading, that is, the sensitivity is largest for RCP2.6 and smallest for RCP8.5. This impact becomes significant after ~2035, as indicated by the gray shading in Figure 6 depicting the range in sensitivity among the four RCP scenarios. The inverse relationship to GHG loading is true for all three vertical regions shown in Figure 6a. The smaller sensitivity under RCP8.5 in the late 21st century is due to the larger CO_2 and N_2O, and much larger CH_4 (by more than a factor of 2) compared to the other three scenarios. This latter point will have a mitigating impact on chlorine-ozone loss via reaction (2). Antarctic spring ozone also has an inverse dependence on GHG loading. However, compared to the large impact due to chlorine, the ozone sensitivity has a relatively small range among the RCP scenarios in Figure 6b and Table 2. Relatively weak Antarctic spring ozone sensitivity to GHG loading was also seen in analysis of the Chemistry-Climate Model Initiative (CCMI) models (Dhomse et al., 2018).

The ozone sensitivity in Figure 6 is also dependent on the decreasing concentrations of bromine-containing source gases (methyl bromide, CH_3Br, and halons) through the 21st century. Decreasing atmospheric bromine will reduce the bromine and chlorine atoms released via the reaction:

$$BrO + ClO \rightarrow Br + Cl + O_2, \quad (3)$$

and this will subsequently reduce the ozone sensitivity to chlorine. To quantify this effect, Figure 6 (magenta line) shows an additional simulation in which atmospheric bromine is held constant at relatively high 2017 levels, with the RCP6.0 scenario used for GHGs. After ~2060, the resulting ozone sensitivity is slightly larger, by 3–5% for global and Antarctic total ozone, compared to the baseline decreasing bromine (black line). This indicates that decreasing bromine has a rather minor impact on the future ozone sensitivity to CFC-11.

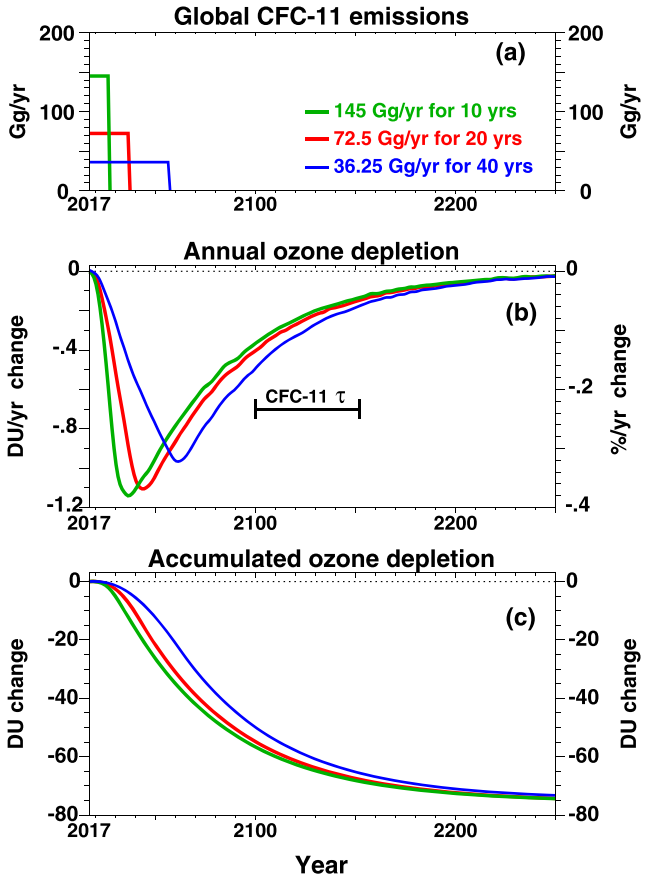

Figure 7. Time series for 2017–2250 showing the (a) global emissions, and (b) annual and (c) accumulated global (90°S–90°N) total ozone depletion for three CFC-11 emission scenarios that have the same total emissions of 1,450 Gg: 145 Gg/year sustained for 10 years (2017–2026) then zero emissions starting in 2027 (green line); 72.5 Gg/year sustained for 20 years (2017–2036) then zero emissions starting in 2037 (red line); and 36.25 Gg/year sustained for 40 years (2017–2056) then zero emissions starting in 2057 (blue line). The ozone depletion is taken as the difference from the zero future CFC-11 emissions scenario starting in 2017 (Figure 1, blue line). The RCP6.0 GHG scenario is used up to 2100. After 2100, all other major ODSs, CO_2, CH_4, and N_2O are held constant at year 2100 values. For reference, the horizontal black bar in Figure 7b depicts the 52-year time scale of the nominal CFC-11 lifetime.

3.4. Impact of Emissions Time Dependence

As illustrated in Figure 6, the ozone depletion for a given level of emissions depends somewhat on the time period over which the ozone depletion is considered. To further examine this point, we compare three future scenarios with identical total CFC-11 emissions, but with different emissions time dependence as shown in Figure 7a: (1) 72.5 Gg/year for 20 years (2017–2036; red line); (2) 145 Gg/year for 10 years (2017–2026; green line), that is, twice the emissions level of (1) for half the time period; and (3) 36.25 Gg/year for 40 years (2017–2056; blue line), that is, half the emissions level of (1) for twice the time period. The RCP6.0 GHG scenario and baseline decreasing bromine are used for all three simulations. Although the total emissions are the same for all three scenarios (1,450 Gg), the time dependence of the ozone response is different. This is shown in Figures 7b and 7c for global total ozone, expressed as the difference from the zero emissions scenario and run out to year 2250 (the results for Antarctic spring ozone are qualitatively similar). For all scenarios, the annual ozone depletion reaches a maximum roughly 5 years after emissions stop (Figure 7b). The ~5-year lag time corresponds roughly to the stratospheric age-of-air and is the time delay between the surface emissions release and subsequent ozone depletion in the stratosphere as discussed in section 3.2. The scenario with the largest emissions early in the time period (145 Gg/year) has the largest accumulated ozone depletion through almost the entire 2017–2250 time period (Figure 7c, green line). However, as the CFC-11 and associated chlorine is removed from the atmosphere, the annual ozone depletion goes to zero and the

accumulated depletion eventually becomes the same in all three scenarios (−74.5 DU). This occurs in the early-mid 2200s, roughly 150–200 years after emissions are stopped, which corresponds to ~3–4 CFC-11 lifetimes (for reference the nominal 52-year CFC-11 lifetime is depicted by the horizontal black bar in Figure 7 b).

These idealized scenarios illustrate that for a given level of cumulative emissions, the shorter-term annual and accumulated ozone depletion will increase as more of the emissions are released earlier in a given time period. However, the long-term accumulated ozone depletion eventually will be independent of the time period of emissions release and will depend mainly on the total amount of CFC-11 emitted, with some dependence on the changing background atmosphere as was discussed in section 3.3.

Finally, we note that the scenarios in Figure 7 correspond to roughly the same level of CFC-11 emitted during the past 20 years (1997–2016, Figure 1a). If this level of emissions were to continue for another 20 years as in Figure 7 (red line), the ozone layer will be impacted well after year 2100 due to the long time scales of the processes involved, with ~30% (22 DU) of the total accumulated depletion occurring after 2100.

4. Conclusions

Increased CFC-11 emissions cause increased stratospheric ozone depletion. In light of the recent increase in global CFC-11 emissions reported in Montzka et al. (2018), we have examined the stratospheric ozone impacts due to emissions potentially continuing into the future. The latitude-height distribution of the ozone response to additional CFC-11 is consistent with that expected due to chlorine perturbations, with the largest percentage changes occurring in the global upper stratosphere and the Antarctic lower stratosphere. Largest total ozone changes occur in the Antarctic spring associated with a deepening ozone hole, although some additional total ozone loss occurs in the southern polar region throughout the year and in the northern polar region during late winter and spring. Qualitatively similar results were obtained in the recent modeling study of Dameris et al. (2019), who found the largest total ozone changes to a CFC-11 perturbation occurred in the Antarctic and Arctic late winter and spring, with generally small changes at midlatitudes and in the tropics.

If the recent increased emissions rapidly decrease back to expected levels in the near future, the ozone impact will be minimal. This is seen in the ozone response to the WMO (2018) baseline scenario that assumed a constant CFC-11 emissions decay rate of 6.4%/year from the present day. This baseline achieves a large emissions reduction by the latter 21st century, as this scenario is nearly equivalent to zero future CFC-11 emissions. However, if emissions remain substantial as in recent years, significant additional ozone depletion will occur, causing a delay in the ozone recovery. For example, sustaining the 2013–2016 average emissions of 72.5 Gg/year out to 2100 will increase EESC by 15% above the baseline. This will result in additional global and Antarctic spring ozone depletion of nearly 1% and 7%, respectively, in 2100, and delay the recovery to 1980 levels by 7.5 and 24.6 years. Furthermore, because of the ~52-year CFC-11 lifetime, time delay between the surface emissions release and ozone loss in the stratosphere, and the long time scale for removal of chlorine from the atmosphere, continuing elevated emissions even for a shorter time period, will impact the stratosphere well into the future. For example, continuing emissions of 72.5 Gg/year, roughly the average during 1997–2016, for another 20 years will cause significant ozone depletion through the mid-21st century, with some impact continuing well beyond 2100.

The calculated future ozone depletion has a strong linear dependence on the cumulative CFC-11 emissions across a wide range of scenarios. Furthermore, sensitivity of additional ozone depletion to the cumulative CFC-11 emissions will depend on the considered time period and future GHG concentrations. GHGs modify the chlorine-related catalytic ozone destruction by direct chemical perturbations and by changes to the radiative properties, temperature, and circulation of the stratosphere. These GHG impacts will also change the CFC-11 lifetime, which will become shorter as GHG levels increase, with a range of ~20% across the RCP scenarios (RCP2.6–RCP8.5). The ozone sensitivity to CFC-11 was found to have a modest inverse dependence on future GHG concentrations, with the largest sensitivity computed under the low GHG loading of the RCP2.6 scenario. The weakest ozone sensitivity was computed under the high RCP8.5 scenario, due in part to the very large CH_4 concentrations in the late 21st century that will reduce the efficiency of the chlorine catalytic ozone destruction. Additionally, the future ozone sensitivity to chlorine will decrease as bromine concentrations decrease, although this impact was found to be relatively minor. Ultimately,

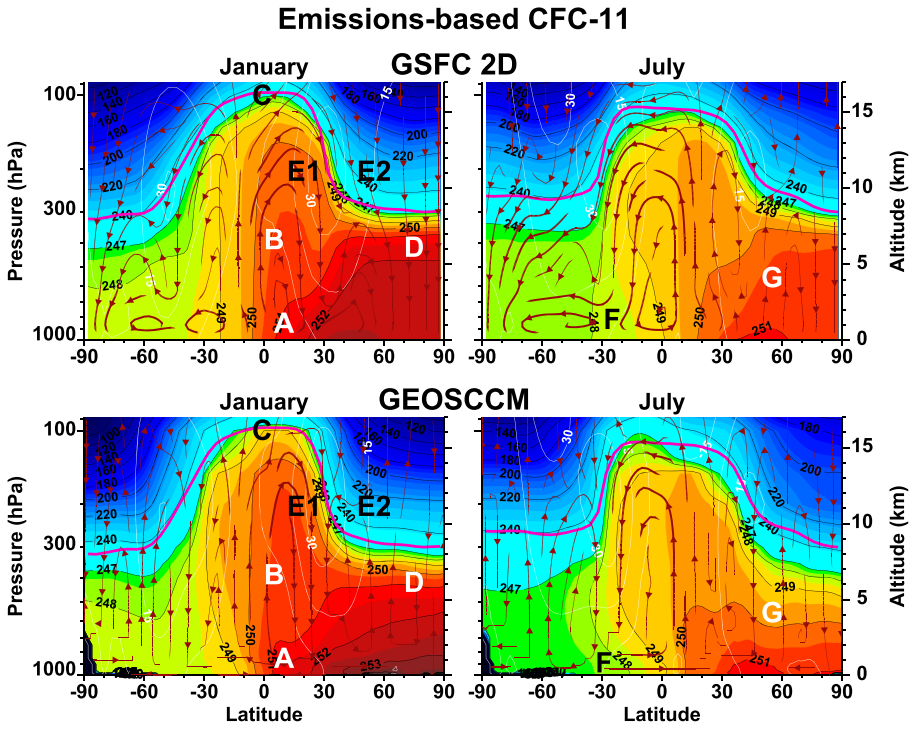

Figure A1. Emissions-based CFC-11 ($CFCl_3$) from GSFC2D (top) and GEOSCCM (bottom) for the January (left) and July (right) average over 2000–2010. Colors show CFC-11 values, with solid black lines in increments of 20 ppt (≤240 ppt) and 1 ppt (≥ 247 ppt). White lines show zonal mean zonal winds at ±15-m/s intervals, while the tropopause is magenta. The brick-colored lines show model streamlines (zonal mean meridional and vertical winds). The letters indicate various transport-sensitive features as described in the text. To facilitate visual comparison between the models, the CFC-11 values have been rescaled so that the global average surface mixing ratio matches that of the observations for 2000–2010 (250 ppt).

however, the total accumulated ozone depletion over the entire life cycle of emissions release to removal of the chlorine from the atmosphere will be determined primarily by the total amount of CFC-11 emitted.

Appendix: GSFC 2D Model Description and Evaluation A.

In this appendix, we provide a description and evaluation of the GSFC2D model used in this work. We compare the GSFC2D baseline simulation with that from the 3-D Goddard Earth Observing System Chemistry-Climate Model (GEOSCCM). The GEOSCCM has a comprehensive tropospheric and stratospheric chemical mechanism (Oman et al., 2016) and performed well in both chemical- and transport-related process evaluations (Douglass et al., 2012, 2014; Eyring et al., 2006; SPARC CCMVal, 2010; Strahan et al., 2011). For reference, we also show total and stratospheric column ozone comparisons with the SPARC CCMI multimodel mean (MMM) (Dhomse et al., 2018) and observational ozone data where available.

GSFC2D has complete stratospheric chemistry but contains a limited subset of tropospheric species (Fleming et al., 2011; Jackman et al., 2016). The model shows good overall agreement with a variety of observations that are sensitive to transport in the meridional plane (e.g., age of air and long-lived tracers), demonstrating that the residual circulation framework used in the model provides a realistic simulation of stratospheric transport on long timescales (>30 days). This is particularly relevant to this study, since stratospheric transport is important for realistic model simulation of atmospheric loss and lifetime of long-lived ODSs including CFC-11 (Chipperfield et al., 2014; Douglass et al., 2008; SPARC, 2013) and model total ozone responses to CFC-11 perturbations.

GSFC2D accounts for long-term CO_2-induced changes in surface temperature (including sea surface temperature), latent heating, and tropospheric water vapor, including the amount of H_2O entering the stratosphere, by parameterizing these quantities using the CO_2 surface boundary condition and sensitivity

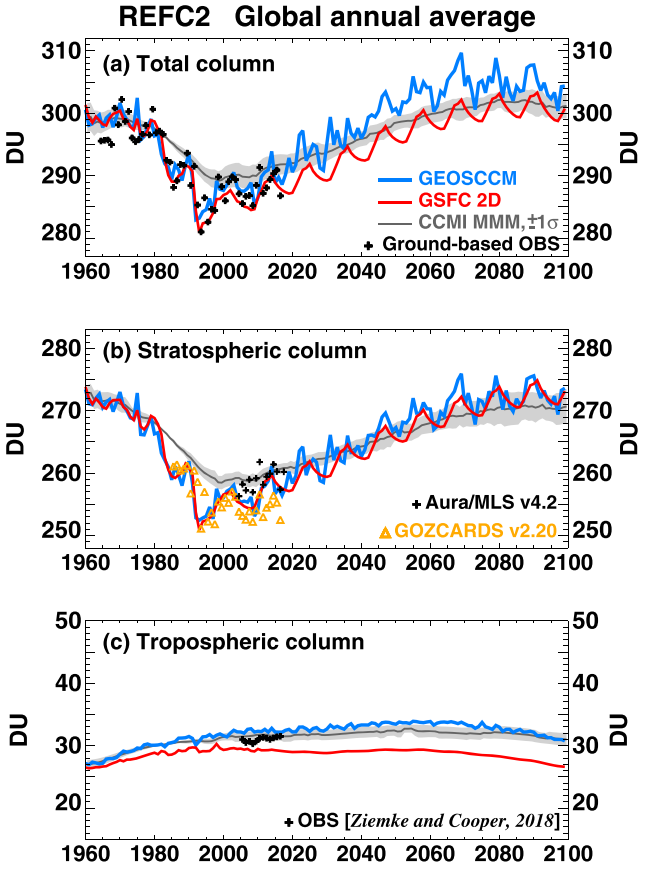

Figure A2. REF-C2 simulations for 1960–2100 and observations of the global (90°S–90°N) and annual average: (a) total column ozone, and the ozone columns (b) above and (c) below the latitude-dependent and seasonally dependent tropopause. Shown are GSFC2D (red line), GEOSCCM (blue line), and the CCMI multimodel mean (MMM, dark gray line with gray shading indicating $\pm 1\sigma$; from Dhomse et al., 2018). The observations are (a) ground-based total ozone for 1964–2017 updated from Fioletov et al. (2002); (b) stratospheric column ozone from Aura/MLS version 4.2 for 2005–2017 (+) and Global OZone Chemistry And Related trace gas Data records for the Stratosphere (GOZCARDS) version 2.20 for 1985–2016, updated from Froidevaux et al. (2015) and time interpolated to fill in missing data (Δ); and (c) tropospheric column ozone derived from OMI/MLS averaged over 60°S to 60°N for 2005–2016 (Ziemke & Cooper, 2017, 2018). To facilitate comparison of the long-term changes and minimize differences in the 1960s, the following offsets were applied: (a) MMM: +5 DU, GEOSCCM: −2 DU; (b) MMM: +12 DU, GEOSCCM: −2 DU, GSFC2D: −1 DU; (c) MMM: −6.5 DU.

factors derived from GEOSCCM simulations. The resulting GSFC2D simulation reproduces the long-term CO_2-induced tropospheric warming, stratospheric cooling, and acceleration of the BDC simulated by the GEOSCCM over the 1950–2100 period (Fleming et al., 2011). Resolving these processes is important to properly simulate long-term changes in ozone and the CFC-11 lifetime. The model kinetic and photolysis rates are updated to the latest JPL-2015 recommendations (Burkholder et al., 2015).

For the GSFC2D model tropospheric transport, large-scale horizontal mixing by synoptic scale eddies is parameterized using orthogonal tracer simulations (Plumb & Mahlman, 1987) performed in the GEOSCCM. Vertical (convective) mixing is based on the convective mass flux obtained from the Modern-Era Retrospective Analysis for Research and Applications reanalysis (Rienecker et al., 2011). The large-scale tropical Hadley circulation is driven largely by the latitudinal and seasonal distribution of latent heating, which is taken from GEOSCCM simulations. The resulting pole-to-pole near-surface age-of-air in GSFC2D (derived from an emissions-based SF_6 simulation) is within ~ ± 5% of observations (Waugh et al., 2013). This gives confidence that the interhemispheric tropospheric transport, which distributes CFC-11 primarily emitted in the NH to the remote SH, is reasonably well simulated by GSFC2D. This is of particular importance for the simulations in this study that are driven by surface CFC-11 emissions.

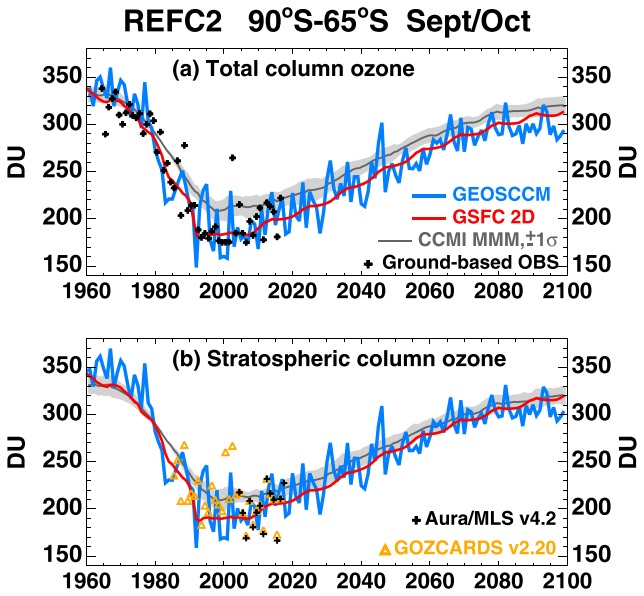

Figure A3. REF-C2 simulations for 1960–2100 and observations of the Antarctic September/October average: (a) total column ozone and (b) stratospheric column ozone (using a latitude-dependent and seasonally dependent tropopause). Shown are GSFC2D (red line), GEOSCCM (blue line), and the CCMI multimodel mean (MMM, dark gray line with gray shading indicating $\pm 1\sigma$; from Dhomse et al., 2018). The observations are (a) ground-based total ozone for 1964–2017 updated from Fioletov et al. (2002); (b) stratospheric column ozone from Aura/MLS version 4.2 for 2005–2017 (+), and Global OZone Chemistry And Related trace gas Data records for the Stratosphere (GOZCARDS) version 2.20 for 1985–2016, updated from Froidevaux et al. (2015) and time interpolated to fill in missing data (Δ). All models in (a) were offset by −30 DU to facilitate long-term comparison with the observations and minimize model-data differences in the 1960s.

An example of emissions-based CFC-11 is shown in Figure A1 for the baseline GSFC2D (top) and GEOSCCM (bottom) simulations for the January (left) and July (right) 2000–2010 average.

The geographical emissions distribution is based on industrial information, with 94% of emissions in the NH and 6% in the SH (Liang et al., 2008; McCulloch et al., 2001). The letters indicate key processes that drive the CFC-11 distribution. Highest CFC-11 concentrations are found in the NH midlatitudes near the surface. During January, the Hadley circulation lower branch advects higher surface concentrations southward ("A" in Figure A1, left). The strong Hadley upward branch and convective mixing lofts these higher concentrations into the upper troposphere ("B"). These higher values are then advected into the stratosphere in the tropics ("C"), where CFC-11 is photolyzed by UV in the lower stratosphere. This CFC-11-depleted air descends into the troposphere in the extratropics ("D"). The subtropical jet stream (between "E1" and "E2") isolates the CFC-11-depleted stratosphere from the CFC-11-rich troposphere. During July, lower CFC-11 concentrations dominate the tropics near the surface as the lower branch of the SH Hadley cell advects air northward ("F" in Figure A1, right). Stronger advection and vertical mixing in the NH summer mixes higher CFC-11 concentrations into the mid-to-upper troposphere ("G"). Additionally, the overall interhemispheric gradient in both January and July is somewhat controlled by large-scale horizontal mixing by synoptic-scale eddies. These features are consistent in both models and illustrate the fidelity of GSFC2D in resolving the overall atmospheric circulation and its seasonal variability in controlling the latitude-height distribution of emissions-based CFC-11.

Figure A2 shows 1960–2100 global ozone from the CCMI baseline REF-C2 simulations from GSFC2D, GEOSCCM, and the CCMI MMM (gray shading indicates $\pm 1\sigma$). These simulations include past stratospheric aerosol variations and solar ultraviolet flux variability associated with the 11-year solar cycle, with a repeating 11-year solar cycle projected out to 2100. The baseline A1 scenario is used for the ODSs (WMO, 2011), and RCP6.0 is used for the GHG mixing ratio boundary conditions (Meinshausen et al., 2011). The GSFC2D stratospheric column ozone agrees quite well with the GEOSCCM, both in absolute amount and pre-2000 decline and future ozone recovery out to 2100 (Figure A2b). While tropospheric column ozone is

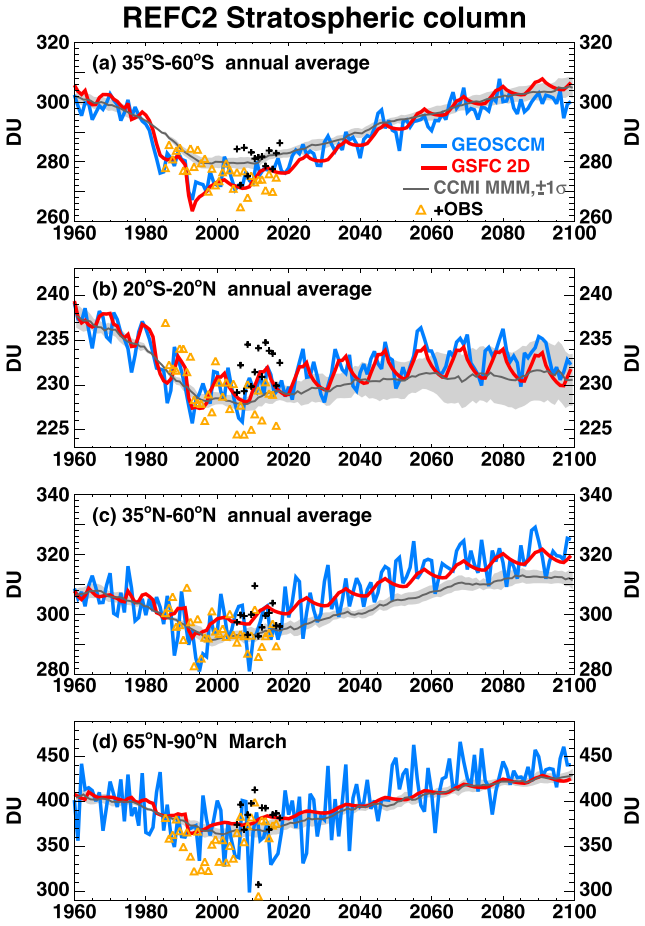

Figure A4. REF-C2 simulations for 1960–2100 and observations of stratospheric column ozone at selected latitude bands (using a latitude-dependent and seasonally dependent tropopause). Observations are from Aura/MLS version 4.2 for 2005–2017 (+) and Global OZone Chemistry And Related trace gas Data records for the Stratosphere (GOZCARDS) version 2.20 for 1985–2016, updated from Froidevaux et al. (2015) and time interpolated to fill in missing data (Δ). To facilitate comparison of the long-term changes and minimize differences in the 1960s, the following offsets were applied: (a) MMM: +12 DU; (b) MMM: +2 DU; (c) MMM: +9 DU, GEOSCCM: −6 DU; (d) MMM: +5 DU, GEOSCCM: −25 DU.

similar in the two models during the 1960s, GSFC2D underestimates the time-dependent increases in tropospheric ozone in the GEOSCCM and MMM from ~1970 through the mid-21st century (Figure A2c). This is likely due to the limited tropospheric chemical scheme used in GSFC2D as mentioned above. This results in a GSFC2D low bias in tropospheric ozone throughout the 21st century, which is as large as 15% (5 DU) in 2050–2060. This low bias is reflected in the total column ozone comparison with GEOSCCM through the 21st century (Figure A2a) and impacts the recovery of global total ozone to 1980 levels. For the REF-C2 simulation, the return date in GSFC2D (2046) is delayed compared with GEOSCCM (2032, after smoothing to remove interannual variability). Although GEOSCCM and GSFC2D show a stronger decline and stronger recovery compared with the CCMI MMM, the GSFC2D recovery date of 2046 is within the uncertainty range of the CCMI models (see Dhomse et al., 2018). Note that because of the different future ODS scenarios and inclusion of stratospheric aerosol and solar cycle variations in REF-C2, the GSFC2D return dates for global and Antarctic spring total ozone cited in this appendix are several years earlier than those listed in Table 1 and shown in Figure 2. For the total and stratospheric column, GSFC2D and GEOSCCM are in overall agreement with the observations. For the tropospheric column, the limited available data fall between GSFC2D and GEOSCCM (see the figure caption for details).

GSFC2D also captures well the decline and recovery of Antarctic spring total and stratospheric column ozone simulated by GEOSCCM (Figure A3), although both models show a somewhat stronger decline

and recovery than the CCMI MMM. For the REF-C2 simulation, the recovery to 1980 total ozone levels occurs in 2062 for both GSFC2D and GEOSCCM, and the CCMI MMM (Dhomse et al., 2018). Note that since the time dependence of Antarctic spring ozone is dominated by the impact of chlorine in the stratosphere, the GSFC2D low bias in tropospheric ozone has a minimal impact on Antarctic total column ozone in Figure A3a.

The GSFC2D low bias in global tropospheric (and total) ozone (Figure A2c) is similar to that at individual latitude zones. To focus on the impact of chlorine perturbations on the stratosphere, Figure A4 shows comparisons at selected latitude zones of stratospheric column ozone. GSFC2D captures well the decline and recovery of stratospheric ozone simulated by GEOSCCM for the tropical and NH and SH midlatitude annual averages. Both models show general agreement with the observations, which have significant year-to-year variability. As with the Antarctic spring comparison (Figure A3), both models show a stronger decline and recovery than the MMM at SH midlatitudes. GSFC2D also compares well with GEOSCCM in simulating the GHG-induced "super recovery" at NH midlatitudes and polar region where stratospheric ozone is 15–30 DU higher in 2100 than in 1960; both models show a larger future increase than the MMM at NH midlatitudes. In addition to declining ODSs, this increase is caused by a combination of stratospheric cooling, which reduces the gas-phase ozone loss rates, and strengthening BDC, which increases the poleward and downward transport of ozone (Langematz & Tully, 2018). GEOSCCM shows large year-to-year variability in the NH, especially in the Arctic where significant ozone loss occurs during cold winters (Figure A4d). As noted in section 3.2, this effect is not captured in the current GSFC2D model, which computes climatologically averaged transport fields. In the tropics, GSFC2D and GEOSCCM show a similar stratospheric ozone decrease during the late 21st century, again driven primarily by GHG changes (Braesicke & Neu, 2018), with both models generally within the fairly large 1σ range of the MMM. These comparisons, therefore, give confidence in the fidelity of the GSFC2D stratospheric and total ozone responses to the CFC-11 perturbations shown in this study.

Acknowledgments
The authors thank Charley Jackman for valuable discussions, and two anonymous reviewers for very helpful comments and suggestions. We thank Luke Oman for supplying the GEOSCCM output and Sandip Dhomse for supplying the CCMI ozone multimodel means used in Appendix A. This work was supported in part by the NASA Headquarters Atmospheric Composition Modeling and Analysis Program. The GSFC2D model description, configuration, input parameters and forcing data sets, and associated references, are provided in section of the main text and in Appendix A. The observational ozone data used for comparisons are available from the following: ground-based total ozone: https://woudc.org/archive/Projects-Campaigns/ZonalMeans/; Aura/MLS: https://disc.gsfc.nasa.gov/datasets?page=1&keywords=AURAMLS; and GOZCARDS: https://gozcards.jpl.nasa.gov/info.php.

References

Bacmeister, J. T., Schoeberl, M. R., Summers, M. E., Rosenfield, J. E., & Zhu, X. (1995). Descent of long-lived trace gases in the winter polar vortex. *Journal of Geophysical Research*, *100*, 11,669–11,684.

Braesicke, P., & Neu, J. (Coordinating lead authors) (2018). Update on global ozone: Past, present and future, chapter 3 of scientific assessment of ozone depletion: 2018, global ozone research and monitoring project, Report No. 58, World Meteorological Organization, Geneva, Switzerland.

Burkholder, J. B, S. P. Sander, J. Abbatt, J. R. Barker, R. E. Huie, C. E. Kolb, et al. (2015). Chemical kinetics and photochemical data for use in atmospheric studies, Evaluation No.18, JPL Publication 15-10, Jet Propulsion Laboratory, Pasadena, (http://jpldataeval.jpl.nasa.gov).

Butchart, N., & Scaife, A. A. (2001). Removal of chlorofluorocarbons by increased mass exchange between the stratosphere and the troposphere in a changing climate. *Nature*, *410*(6830), 799–802. https://doi.org/10.1038/35071047

Carpenter, L. J., & Daniel, J. S. (Coordinating lead authors) (2018). Scenarios and information for policymakers, chapter 6 of scientific assessment of ozone depletion: 2018, global ozone research and monitoring project, Report No.58, World Meteorological Organization, Geneva, Switzerland.

Chipperfield, M. P., Liang, Q., Strahan, S. E., Morgenstern, O., Dhomse, S. S., Abraham, N. L., et al. (2014). Multi-model estimates of atmospheric lifetimes of long-lived ozone-depleting substances: Present and future. *Journal of Geophysical Research: Atmospheres*, *119*, 2555–2573. https://doi.org/10.1002/2013JD021097

Considine, D. B., Douglass, A. R., & Jackman, C. H. (1994). Effects of a polar stratospheric cloud parameterization on ozone depletion due to stratospheric aircraft in a two-dimensional model. *Journal of Geophysical Research*, *99*(D9), 18,879–18,894. https://doi.org/10.1029/94JD01026

Cunnold, D. M., Weiss, R. F., Prinn, R. G., Hartley, D., Simmonds, P. G., Fraser, P. J., et al. (1997). GAGE/AGAGE measurements indicating reductions in global emissions of CCl_3F and CCl_2F_2 in 1992-1994. *Journal of Geophysical Research*, *102*(D1). https://doi.org/10.1029/96JD02973

Dameris, M., & Godin-Beekmann, S. (Coordinating lead authors) (2014). Update on polar ozone: Past, present and future, chapter 3 of scientific assessment of ozone depletion: 2014, global ozone research and monitoring project, Report No. 55, World Meteorological Organization, Geneva, Switzerland.

Dameris, M., Jöckel, P., & Nützel, M. (2019). Possible implications of enhanced chlorofluorocarbon-11 concentrations on ozone. *Atmospheric Chemistry and Physics*, *19*, 13,759–13,771. https://doi.org/10.5194/acp-19-13759-2019

Dhomse, S. S., Kinnison, D., Chipperfield, M. P., Salawitch, R. J., Cionni, I., Hegglin, M. I., et al. (2018). Estimates of ozone return dates from chemistry-climate model initiative simulations. *Atmospheric Chemistry and Physics*, *18*(11), 8409–8438. https://doi.org/10.5194/acp-18-8409-2018

Douglass, A. R., Stolarski, R., Jackman, C., Gupta, M., Newman, P., Nielsen, J., & Fleming, E. (2008). Relationship of loss, mean age of air and the distribution of CFCs to stratospheric circulation and implications for atmospheric lifetimes. *Journal of Geophysical Research*, *113*, D14309. https://doi.org/10.1029/2007JD009575

Douglass, A. R., Stolarski, R. S., Strahan, S. E., & Oman, L. D. (2012). Understanding differences in upper stratospheric ozone response to changes in chlorine and temperature as computed using CCMVal-2 models. *Journal of Geophysical Research*, *117*, D16306. https://doi.org/10.1029/2012JD017483

Douglass, A. R., Strahan, S. E., Oman, L. D., & Stolarski, R. S. (2014). Understanding differences in chemistry climate model projections of stratospheric ozone. *Journal of Geophysical Research: Atmospheres*, *119*, 4922–4939. https://doi.org/10.1002/2013JD021159

Engel, A., & Rigby, M. (Coordinating lead authors) (2018). Update on ozone-depleting substances (ODSs) and other gases of interest to the montreal protocol, chapter 1 of scientific assessment of ozone depletion: 2018, global ozone research and monitoring project, Report No.58, World Meteorological Organization, Geneva, Switzerland.

Eyring, V., Butchart, N., Waugh, D. W., Akiyoshi, H., Austin, J., Bekki, S., et al. (2006). Assessment of temperature, trace species, and ozone in chemistry-climate model simulations of the recent past. *Journal of Geophysical Research*, *111*, D22308. https://doi.org/10.1029/2006JD007327

Fioletov, V. E., Bodeker, G. E., Miller, A. J., McPeters, R. D., & Stolarski, R. (2002). Global ozone and zonal total ozone variations estimated from ground-based and satellite measurements, *Journal of Geophysical Research*, *107*(D22), 4647. https://doi.org/10.1029/2001JD001350

Fleming, E. L., George, C., Heard, D. E., Jackman, C. H., Kurylo, M. J., Mellouki, W., et al. (2015). The impact of current CH_4 and N_2O atmospheric loss process uncertainties on calculated ozone abundances and trends. *Journal of Geophysical Research: Atmospheres*, *120*, 5267–5293. https://doi.org/10.1002/2014JD022067

Fleming, E. L., Jackman, C. H., Stolarski, R. S., & Douglas, A. R. (2011). A model study of the impact of source gas changes on the stratosphere for 1850–2100. *Atmospheric Chemistry and Physics*, *11*(16), 8515–8541. https://doi.org/10.5194/acp-11-8515-2011

Fleming, E. L., Jackman, C. H., Weisenstein, D. K., & Ko, M. K. W. (2007). The impact of inter-annual variability on multidecadal total ozone simulations. *Journal of Geophysical Research*, *112*, D10310. https://doi.org/10.1029/2006JD007953

Froidevaux, L., Anderson, J., Wang, H.-J., Fuller, R. A., Schwartz, M. J., Santee, M. L., et al. (2015). Global OZone Chemistry and Related trace gas Data records for the Stratosphere (GOZCARDS): Methodology and sample results with a focus on HCl, H_2O, and O_3, *Atmospheric Chemistry and Physics*, *15*, 10,471–10,507. https://doi.org/10.5194/acp-15-10471-2015

Haigh, J. D., & Pyle, J. A. (1979). A two-dimensional calculation including atmospheric carbon dioxide and stratospheric ozone, *Nature*, *279*, 222–224.

Jackman, C. H., Fleming, E. L., Chandra, S., Considine, D. B., & Rosenfield, J. E. (1996). Past, present, and future modeled ozone trends with comparisons to observed trends. *Journal of Geophysical Research*, *101*(D22), 28,753–28,767.

Jackman, C. H., Marsh, D. R., Kinnison, D. E., Mertens, C. J., & Fleming, E. L. (2016). Atmospheric changes caused by galactic cosmic rays over the period 1960–2010. *Atmospheric Chemistry and Physics*, *16*, 5853–5866. https://doi.org/10.5194/acp-16-5853-2016

Karpechko, A. Yu., & Maycock, A. C. (Coordinating lead authors) (2018). Stratospheric ozone changes and climate, chapter 5 of scientific assessment of ozone depletion: 2018, global ozone research and monitoring project, Report No.58, World Meteorological Organization, Geneva, Switzerland.

Keeble, J., Abraham, N. L., Archibald, A. T., Chipperfield, M. P., Dhomse, S., Griffiths, P. T., & Pyle, J. A. (2019). Modelling the potential impacts of the recent, unexpected increase in CFC-11 emissions on total column ozone recovery. *Atmospheric Chemistry and Physics Discussions*. https://doi.org/10.5194/acp-2019-747

Langematz, U., & Tully, M. (Coordinating lead authors) (2018). Polar stratospheric ozone: Past, present and future, chapter 4 of scientific assessment of ozone depletion: 2018, global ozone research and monitoring project, Report No. 58, World Meteorological Organization, Geneva, Switzerland.

Liang, Q., Stolarski, R. S., Douglass, A. R., Newman, P. A., & Nielsen, J. E. (2008). Evaluation of emissions and transport of CFCs using surface observations and their seasonal cycles and simulation of the GEOS CCM with emissions-based forcing. *Journal of Geophysical Research*, *113*, D14302. https://doi.org/10.1029/2007JD009617

McCulloch, A., Ashford, P., & Midgley, P. M. (2001). Historic emissions of fluorotrichloromethane (CFC-11) based on a market survey. *Atmospheric Environment*, *35*(26), 4387–4397.

Meinshausen, M., Smith, S. J., Calvin, K., Daniel, J. S., Kainuma, M. L. T., Lamarque, J.-F., et al. (2011). The RCP greenhouse gas concentrations and their extensions from 1765 to 2300. *Climatic Change*, *109*, 213–241. https://doi.org/10.1007/s10584-011-0156-z

Montzka, S. A., Dutton, G. S., Yu, P., Ray, E., Portmann, R. W., Daniel, J. S., et al. (2018). An unexpected and persistent increase in global emissions of ozone-depleting CFC-11. *Nature*, *557*(7705), 413–417. https://doi.org/10.1038/s41586-018-0106-2

Newman, P. A., Daniel, J. S., Waugh, D. W., & Nash, E. R. (2007). A new formulation of equivalent effective stratospheric chlorine (EESC). *Atmospheric Chemistry and Physics*, *7*(17), 4537–4552. https://doi.org/10.5194/acp-7-4537-2007

Oman, L. D., Douglass, A. R., Salawitch, R. J., Canty, T. P., Ziemke, J. R., & Manyin, M. (2016). The effect of representing bromine from VSLS on the simulation and evolution of Antarctic ozone. *Geophysical Research Letters*, *43*, 9869–9876. https://doi.org/10.1002/2016GL070471

Pawson, S., & Steinbrecht, W. (Coordinating lead authors) (2014). Update on global ozone: Past, present and future, chapter 2 of scientific assessment of ozone depletion: 2014, global ozone research and monitoring project, Report No. 55, World Meteorological Organization, Geneva, Switzerland.

Plumb, R. A., & Mahlman, J. D. (1987). The zonally averaged transport characteristics of the GFDL general circulation/transport model. *Journal of the Atmospheric Sciences*, *44*, 298–327.

Prinn, R. G., Weiss, R. F., Arduini, J., Arnold, T., DeWitt, H. L., Fraser, P. J., et al. (2018). History of chemically and radiatively important atmospheric gases from the Advanced Global Atmospheric Gases Experiment (AGAGE). *Earth System Science Data*, *10*(2), 985–1018. https://doi.org/10.5194/essd-10-985-2018

Revell, L. E., Stenke, A., Rozanov, E., Ball, W., Lossow, S., & Peter, T. (2016). The role of methane in projections of 21st century stratospheric water vapour. *Atmospheric Chemistry and Physics*, *16*, 13,067–13,080. https://doi.org/10.5194/acp-16-13067-2016

Rienecker, M. M., Suarez, M. J., Gelaro, R., Todling, R., Bacmeister, J., Liu, E., et al. (2011). MERRA: NASA's Modern-Era Retrospective Analysis for Research and Applications. *Journal of Climate*, *24*(14), 3624–3648. https://doi.org/10.1175/JCLI-D-11-00015.1

Rigby, M., Park, S., Saito, T., Western, L. M., Redington, A. L., Fang, X., et al. (2019). Increase in CFC-11 emissions from eastern China based on atmospheric observations. *Nature*, *569*(7757), 546–550. https://doi.org/10.1038/s41586-019-1193-4

Rosenfield, J. E., Considine, D. B., Meade, P. E., Bacmeister, J. T., Jackman, C. H., & Schoeberl, M. R. (1997). Stratospheric effects of Mount Pinatubo aerosol studied with a coupled two-dimensional model. *Journal of Geophysical Research*, *102*, 3649–3670.

Rosenfield, J. E., Douglass, A. R., & Considine, D. B. (2002). The impact of increasing carbon dioxide on ozone recovery. *Journal of Geophysical Research*, *107*(D6), 4049. https://doi.org/10.1029/2001JD000824

Smalley, K. M., Dessler, A. E., Bekki, S., Deushi, M., Marchand, M., Morgenstern, O., et al. (2017). Contribution of different processes to changes in tropical lower-stratospheric water vapor in chemistry-climate models. *Atmospheric Chemistry and Physics*, *17*(13), 8031–8044. https://doi.org/10.5194/acp-17-8031-2017

SPARC (2013). The lifetimes of stratospheric ozone-depleting substances, their replacements, and related species, SPARC Rep. 6, WCRP-15/2013, edited by M. Ko et al., SPARC Office, Zurich, Switzerland.

SPARC CCMVal (Stratosphere-troposphere processes and their role in climate), (2010). SPARC Report on the Evaluation of Chemistry-Climate Models, edited by V. Eyring, T.G. Shepherd, and D.W. Waugh, SPARC Report No. 5, WCRP-132, WMO/TD-No. 1526, 478 pp., available: http://www.atmosp.physics.utoronto.ca/SPARC/ccmval_final/index.php.

Strahan, S. E., Douglass, A. R., Stolarski, R. S., Akiyoshi, H., Bekki, S., Braesicke, P., et al. (2011). Using transport diagnostics to understand chemistry climate model ozone simulations. *Journal of Geophysical Research*, *116*, D17302. https://doi.org/10.1029/2010JD015360

Velders, G. J. M., & Daniel, J. S. (2014). Uncertainty analysis of projections of ozone-depleting substances: Mixing ratios, EESC, ODPs, and GWPs. *Atmospheric Chemistry and Physics*, *14*(6), 2757–2776. https://doi.org/10.5194/acp-14-2757-2014

Waugh, D. W., Crotwell, A. M., Dlugokencky, E. J., Dutton, G. S., Elkins, J. W., Hall, B. D., et al. (2013). Tropospheric SF_6: Age of air from the Northern Hemisphere midlatitude surface. *Journal of Geophysical Research: Atmospheres*, *118*, 11,429–11,441. https://doi.org/10.1002/jgrd.50848

WMO (1999). Scientific assessment of ozone depletion: 1998, global ozone research and monitoring project, *Rep. 44*, World Meteorological Organization, Geneva, Switzerland.

WMO (2011). Scientific assessment of ozone depletion: 2010, global ozone research and monitoring project, Report No. 52, World Meteorological Organization, Geneva, Switzerland.

WMO (2018). Scientific assessment of ozone depletion: 2018, global ozone research and monitoring project, Report No. 58, World Meteorological Organization, Geneva, Switzerland.

Ziemke, J. R., & Cooper, O. R. (2017). Tropospheric ozone, state of the climate in 2016. *Bulletin of the American Meteorological Society*, *98*, S52–S54. https://doi.org/10.1175/2017BAMSStateof-Climate.1

Ziemke, J. R., & Cooper, O. R. (2018). Tropospheric ozone, state of the climate in 2017. *Bulletin of the American Meteorological Society*, *99*(8). https://doi.org/10.1175/2018BAMSStateof-Climate.1